HAL
open science

Numerical boundary conditions in Finite Volume and Discontinuous Galerkin schemes for the simulation of rarefied flows along solid boundaries

Céline Baranger, Nicolas Hérouard, Julien Mathiaud, Luc Mieussens

To cite this version:

Céline Baranger, Nicolas Hérouard, Julien Mathiaud, Luc Mieussens. Numerical boundary conditions in Finite Volume and Discontinuous Galerkin schemes for the simulation of rarefied flows along solid boundaries. Mathematics and Computers in Simulation, 2019, 159, pp.136-153. 10.1016/j.matcom.2018.11.011 . hal-01552756v4

HAL Id: hal-01552756

https://hal.science/hal-01552756v4

Submitted on 12 Mar 2020

HAL is a multi-disciplinary open access archive for the deposit and dissemination of scientific research documents, whether they are published or not. The documents may come from teaching and research institutions in France or abroad, or from public or private research centers.

L'archive ouverte pluridisciplinaire **HAL**, est destinée au dépôt et à la diffusion de documents scientifiques de niveau recherche, publiés ou non, émanant des établissements d'enseignement et de recherche français ou étrangers, des laboratoires publics ou privés.

Numerical boundary conditions in Finite Volume and Discontinuous Galerkin schemes for the simulation of rarefied flows along solid boundaries

C. Baranger[1], N. Hérouard[1,2], J. Mathiaud[1,2], L. Mieussens[2]

[1]CEA-CESTA
15 avenue des Sablières - CS 60001
33116 Le Barp Cedex, France
(celine.baranger@cea.fr, julien.mathiaud@cea.fr)

[2] Bordeaux INP, Univ. Bordeaux, CNRS, INRIA, IMB, UMR 5251, F-33400 Talence, France.
(Nicolas.Herouard@math.u-bordeaux.fr, Luc.Mieussens@math.u-bordeaux.fr)

Abstract: We present a numerical comparison between two standard finite volume schemes and a discontinuous Galerkin method applied to the BGK equation of rarefied gas dynamics. We pay a particular attention to the numerical boundary conditions in order to preserve the rate of convergence of the method. Most of our analysis relies on a 1D problem (Couette flow), but we also present some results for a 2D aerodynamical flow.

Keywords: rarefied flow simulation, BGK model, Finite Volume Schemes, Discontinuous Galerkin schemes, Numerical boundary conditions

Contents

1 Introduction **2**

2 The BGK equation **3**

3 Numerical schemes and boundary conditions **5**

3.1 Finite Volume schemes 5

3.1.1 A first order scheme finite volume scheme 6

3.1.2 Second order finite volume scheme with flux limiters 7

3.1.3 Second order finite volume second order scheme based on linear reconstruction 8

3.2 Discontinuous Galerkin scheme 11

3.2.1 Weak form and piecewise linear approximation 12

3.2.2 Time discretization 13

3.2.3 Boundary conditions 14

4 Numerical results **14**
4.1 Test-case and reduced model in 1D: Couette flow 14
4.2 Comparison of second order Finite Volume schemes on the 1D Couette flow . 15
4.3 Validation of the Finite Volume scheme in 2D 16
4.4 Comparison between the Discontinuous Galerkin and Finite Volume schemes 17

5 Conclusions and perspectives **18**

1 Introduction

The kinetic theory of Rarefied gas flows describes the behavior of a gas in a system which length is of same order of magnitude as the mean free path of the gas molecules. Numerical simulations of these flows are fundamental tools, for instance they are used in aerodynamics to estimate heat fluxes at the surface of a re-entry space vehicle at high altitudes or to estimate the attenuation of a micro-accelerometer by the surrounding gas in a micro-electro-mechanical system. One last example is when one wants to estimate the pumping speed or compression rate of a turbo-molecular pump.

For such problems, it is important to take into account the interactions of the gas with the solid boundaries of the system. They are modeled by boundary conditions like the diffuse or specular reflections. In this work, our first aim is to improve the accuracy of our in-house kinetic solver, which is based on a finite volume approach (FV), in particular for the computation of parietal fluxes. Finite volume schemes are often used in rarefied gas dynamics (RGD), see for instance the work of [20, 15, 1, 9, 22]. Our scheme uses a standard extension to second order accuracy by using the non linear flux limiter approach of Yee [23]. We observe that the accuracy of this scheme decreases to first order at solid boundaries, because the boundary conditions are not discretized properly. The first goal of this paper is to analyze this problem, both analytically and numerically. We show that our flux limiter can hardly be compatible with second order discretization of reflection boundary conditions.

Then we study another kind of second order extension based on linear reconstruction and nonlinear slope limiters [13]. In this case, we are able to propose a discretization of the boundary conditions (inspired by [11, 8]), based on extrapolations that are consistent with the slope limiter technique, which preserves second order accuracy up to solid boundaries. On numerical tests, the improvement of the accuracy of this method is spectacular, for 1D and 2D problems.

Finally, we want to compare this modified finite volume scheme to the popular Discontinuous Galerkin method (DG). Incidentally, this method has originally been made for neutron transport (hence a kinetic equation, like the Boltzmann equation of RGD) in the 1970's by Reed and Hill [18]. Such schemes have many interesting properties, and they became more and more popular in the past decades in many different fields. In particular, the DG method has been used for charged particles [5], and more recently for the BGK equation [19]. According to this last paper, the DG method would be more efficient that the FV method, at least for the test cases used by the authors. In this paper, we show that the discretization of

reflection conditions with a DG method is very simple. We compare a simple second order DG scheme to our two FV schemes, mainly to investigate their accuracy at solid boundaries. This study shows the order of accuracy of both DG and FV method (with slope limiters) are not decreased at solid boundaries.

The outline of this article is the following. In section 2, we present the basic BGK equation of RGD. In 3, we analyze the two versions of our FV scheme and a simple DG scheme. These schemes are compared for several test cases in section 4.

2 The BGK equation

In kinetic theory, a monoatomic gas is described by a particle distribution function $f(t, \mathbf{x}, \mathbf{v})$ defined such as $f(t, \mathbf{x}, \mathbf{v})\mathrm{d}\mathbf{x}\mathrm{d}\mathbf{v}$ is the mass of molecules that at time t are located in an elementary space volume $d\mathbf{x}$ centered in $\mathbf{x} = (x, y, z)$ and have a velocity in an elementary volume $d\mathbf{v}$ centered in $\mathbf{v} = (v_x, v_y, v_z)$. The macroscopic quantities associated to f such as mass density ρ, momentum $\rho\mathbf{u}$ and total energy E are defined as the five first moments of f with respect to the velocity variable, namely:

$$(\rho(t, \mathbf{x}), \rho\mathbf{u}(t, \mathbf{x}), E(t, \mathbf{x})) = \int_{\mathbb{R}^3} (1, \mathbf{v}, \frac{1}{2}|\mathbf{v}|^2) f(t, \mathbf{x}, \mathbf{v})\, \mathrm{d}\mathbf{v}. \tag{1}$$

The temperature T of the gas and its pressure $p = \rho RT$ are defined by the relation

$$E = \frac{1}{2}\rho|\mathbf{u}|^2 + \frac{3}{2}\rho RT \tag{2}$$

where R is the gas constant defined as the ratio between the Boltzmann constant and the molecular mass of the gas. When the gas is in a thermodynamical equilibrium state, it is well known that the distribution function f is a Gaussian function $M[\rho, \mathbf{u}, T]$ of $\mathbf{v}$, called Maxwellian distribution, that depends only on macroscopic quantities and satisfies relations (1):

$$M[\rho, \mathbf{u}, T] = \frac{\rho}{(2\pi RT)^{\frac{3}{2}}} \exp(-\frac{|\mathbf{v} - \mathbf{u}|^2}{2RT}). \tag{3}$$

The evolution of a gas at thermodynamical nonequilibrium is described by the following Boltzmann equation:

$$\partial_t f + \mathbf{v} \cdot \nabla_{\mathbf{x}} f = Q(f), \tag{4}$$

which means that the total variation of f (described by the left-hand side) is due to collisions between molecules ($Q(f)$ is the collision kernel). The most realistic collision kernel is the Boltzmann operator but its use is still very computationally expensive. Here we choose the simpler BGK model [2, 21]

$$Q(f) = \frac{1}{\tau}(M[\rho, \mathbf{u}, T] - f) \tag{5}$$

which makes f relax towards the local equilibrium corresponding to the macroscopic quantities defined by (1). The relaxation time defined as $\tau = \dfrac{\mu}{\rho RT}$ (μ being the viscosity of

the gas) is chosen to recover the correct viscosity in the Chapman-Enskog expansion for Navier-Stokes equations.

The interactions of the gas with solid boundaries are described with a diffuse reflection model. If the boundary has a temperature T_w and a velocity $\mathbf{u}_w$ so that $\mathbf{u}_w \cdot \mathbf{n}(\mathbf{x}) = 0$, where $\mathbf{n}(\mathbf{x})$ is the normal to the wall at point $\mathbf{x}$ directed into the gas, a molecule that collides with the boundary is re-emitted with a random velocity normally distributed around $\mathbf{u}_w$ (RT_w being the variance of the normal distribution). This reads

$$f(t, \mathbf{x}, \mathbf{v})_{|\Gamma} = \sigma_w(f) M[1, \mathbf{u}_w, T_w](\mathbf{v}) \quad \text{if } \mathbf{v} \cdot \mathbf{n}(\mathbf{x}) > 0. \tag{6}$$

The parameter $\sigma_w(f)$ is the mass density of reflected particles, and it is defined so that there is no normal mass flux across the boundary (all the molecules are re-emitted), see [4]. Namely, that is,

$$\sigma_w(f) = -\left(\int_{\mathbf{v}\cdot\mathbf{n}(\mathbf{x})<0} \mathbf{v} \cdot \mathbf{n}(\mathbf{x}) f(t, \mathbf{x}, \mathbf{v}) \, \mathrm{d}\mathbf{v} \right) \left(\int_{\mathbf{v}\cdot\mathbf{n}(\mathbf{x})>0} \mathbf{v} \cdot \mathbf{n}(\mathbf{x}) M[1, \mathbf{u}_w, T_w](\mathbf{v}) \, \mathrm{d}\mathbf{v} \right)^{-1}. \tag{7}$$

There are other reflection models, like the Maxwell model with partial accommodation, but they are not used in this work.

The numerical resolution of the BGK equation is done by a deterministic method using a discrete velocity approach (see [15, 16, 17], and the extension to polyatomic gases [10]). The velocity variable is replaced by discrete values $\mathbf{v}_k$ of a Cartesian grid (see [1] for the use of locally refined velocity grids). The continuous distribution f is then replaced by its approximation at each point $\mathbf{v}_k$, and we get the following discrete velocity BGK equation

$$\frac{\partial f_k}{\partial t} + \mathbf{v}_k \cdot \nabla_{\mathbf{x}} f_k = \frac{1}{\tau} (\mathcal{M}_k[\rho, \mathbf{u}, T] - f_k), \tag{8}$$

where $f_k(t, \mathbf{x}) \approx f(t, \mathbf{x}, \mathbf{v}_k)$. The discrete function $\mathcal{M}_k$ is an approximation of the equilibrium functions M defined in (3) at point $\mathbf{v}_k$. This discrete equilibrium is defined in order to satisfy the conservation of mass, momentum and energy (see [15]). The macroscopic quantities are now defined by the quadrature rule

$$(\rho(t, \mathbf{x}), \rho \mathbf{u}(t, \mathbf{x}), E(t, \mathbf{x})) = \sum_k (1, \mathbf{v}_k, \frac{1}{2} |\mathbf{v}_k|^2) f_k(t, \mathbf{x}) \, \omega_k, \tag{9}$$

where ω_k are the quadrature weights: for a Cartesian velocity grid of steps Δv_x, Δv_y, Δv_z, the weights are given by $\omega_k = \Delta v_x \Delta v_y \Delta v_z$. Moreover, the boundary condition (6) is replaced by

$$f_k(t, \mathbf{x})_{|\Gamma} = \sigma_w(f) \mathcal{M}_k[1, \mathbf{u}_w, T_w] \quad \text{if } \mathbf{v}_k \cdot \mathbf{n}(\mathbf{x}) > 0, \tag{10}$$

where $\sigma_w(f)$ is defined as in (7) in which the integrals are replaced by quadratures:

$$\sigma_w(f) = -\left(\sum_{\mathbf{v}_k\cdot\mathbf{n}(\mathbf{x})<0} \mathbf{v}_k \cdot \mathbf{n}(\mathbf{x}) f_k(t, \mathbf{x}) \, \omega_k \right) \left(\sum_{\mathbf{v}_k\cdot\mathbf{n}(\mathbf{x})>0} \mathbf{v}_k \cdot \mathbf{n}(\mathbf{x}) \mathcal{M}_k[1, \mathbf{u}_w, T_w] \, \omega_k \right)^{-1}. \tag{11}$$

Again this ensures a zero mass flux across the solid wall.

3 Numerical schemes and boundary conditions

For the sake of simplicity, the numerical scheme will be presented in the 1D configuration, in the domain $[0, 1]$. Equation (8) is then written

$$\frac{\partial f_k}{\partial t} + v_k \frac{\partial f_k}{\partial x} = \frac{1}{\tau}(\mathcal{M}_k[\rho, \mathbf{u}, T] - f_k), \tag{12}$$

where v_k is the first component of $\mathbf{v}_k$. Since $\mathbf{v}_k \cdot \mathbf{n}(\mathbf{x}) = v_k$ (at $x = 0$), the boundary condition (10)–(11) now reads

$$f_k(t, 0) = \sigma_w(f)\mathcal{M}_k[1, \mathbf{u}_w, T_w] \;\text{ if } v_k > 0, \tag{13}$$

where

$$\sigma_w(f) = -\left(\sum_{v_k<0} v_k f_k(t, 0)\,\omega_k\right)\left(\sum_{v_k>0} v_k \mathcal{M}_k[1, \mathbf{u}_w, T_w]\,\omega_k\right)^{-1}. \tag{14}$$

For the following, it is important to note that boundary condition (13)–(14) implies a zero mass flux ϕ at the boundary. Indeed, (13) yields:

$$\begin{aligned}\phi &:= \sum_k v_k f_k(t, 0)\,\omega_k \\ &= \sum_{v_k<0} v_k f_k(t, 0)\,\omega_k + \sum_{v_k<0} v_k \sigma_w(f)\mathcal{M}_k[1, \mathbf{u}_w, T_w]\,\omega_k = 0\end{aligned}$$

from (14). In particular, this property ensures a global mass conservation for any internal flow.

3.1 Finite Volume schemes

Finite Volume schemes approximate the solution of a given problem by integrating the equation on each cell of a mesh. The integration of the advection term results in a flux at cell interfaces: the numerical flux. The accuracy of the scheme depends on the accuracy of this flux. Moreover, this flux is closely linked with the boundary conditions. This is why, in this section, we study in detail three different finite volume schemes and their properties close to a solid boundary. Note that the collision term $Q(f)$ is local in space and its discretization is consequently the same for all Finite Volume schemes: therefore, even if we take the BGK equation as an example, the study performed in this section can be applied to every collision operator.

First, we assume we have a mesh of $i_{max}+1$ nodes $x_{i+\frac{1}{2}}$ with steps $\Delta x_i = x_{i+\frac{1}{2}} - x_{i-\frac{1}{2}}$, for $i = 1$ to $i = i_{max}$. The discrete time variable is t_n with a time step Δt_n. We first integrate equation (12) in a cell $[x_{i-\frac{1}{2}}, x_{i+\frac{1}{2}}]$ between t_n and t_{n+1} and divide by Δt_n to obtain

$$\frac{f_{i,k}^{n+1} - f_{i,k}^n}{\Delta t_n} + \frac{1}{\Delta x_i}\left(\mathcal{F}^n_{i+\frac{1}{2},k} - \mathcal{F}^n_{i-\frac{1}{2},k}\right) = Q_k(f_i^n), \tag{15}$$

where $f^n_{i,k}$ is an approximation of the average of $f_k(t_n, x)$ in the cell i. The numerical flux $\mathcal{F}^n_{i+\frac{1}{2},k}$ is an approximation of the integral $\int_{t^n}^{t^{n+1}} v_k f_k(t, x_{i+\frac{1}{2}})\, dt$, and can be interpreted as a flux across the cell interface $x_{i+\frac{1}{2}}$ between cells i and $i+1$.

In the literature, there are many different constructions of this numerical flux, and each one leads to a different scheme. The simplest one is the upwind scheme (see section 3.1.1 below), which gives a first order scheme. There are several ways to increase the order of a this scheme, all of them related to a modification of the numerical flux. One solution is to reconstruct the solution inside the cells of the mesh, in order to define new values on the interfaces. Another one is to limit a high order numerical flux at the cell interfaces. Here, we study one method of each category, and in particular their properties at the solid boundary. We first present the standard first order upwind scheme. Then we study a second order flux limiter method and show it decreases to first order at the boundary. Then we present the linear reconstruction method, which gives a correct second-order approximation of the BGK problem up to the boundary.

Finally, note that, for simplicity, all our schemes are presented with a standard forward (explicit) Euler time discretization. In practice, since we are interested in steady flows only, our numerical tests are made with a linearized backward (implicit) Euler method, which is standard in aerodynamics (see [15, 1]). However, the analysis made below does not depend on the time discretization.

3.1.1 A first order scheme finite volume scheme

The simplest numerical flux is the upwind flux:

$$\mathcal{F}^n_{i+\frac{1}{2},k} = v_k^+ f^n_{i,k} + v_k^- f^n_{i+1,k},$$

where $v_k^\pm = (v \pm |v|)/2$ denotes the positive and negative parts of v_k. It is well known that the corresponding scheme is first order accurate in space, with a strong numerical diffusion on coarse meshes.

Assume that the first cell of the mesh $[x_{\frac{1}{2}}, x_{\frac{3}{2}}]$ is adjacent to a solid wall. Then the numerical flux $\mathcal{F}^n_{\frac{1}{2},k}$ approximates the flux across the solid boundary. It requires an artificial value $f^n_{0,k}$, that is generally interpreted as the value of the distribution function in a *ghost cell* $[x_{-\frac{1}{2}}, x_{\frac{1}{2}}]$ inside the solid wall, adjacent to the first cell. This value must be defined so as to (a) account for the boundary condition (13)–(14), and (b) satisfy a zero mass flux across the wall, that is to say $\sum_k \mathcal{F}^n_{\frac{1}{2},k}\omega_k = 0$.

These constraints can be satisfied as follows. First, the value of $f^n_{0,k}$ is defined for outgoing velocities $v_k < 0$ by using a zeroth order extrapolation of the value in Ω_1, namely

$$f^n_{0,k} = f^n_{1,k}.$$

Then, the value of $f^n_{0,k}$ for incoming velocities is defined by using the boundary condition (13-14), that is to say:

$$f^n_{0,k} = \sigma_w(f^n_0)\mathcal{M}_k[1, \mathbf{u}_w, T_w], \quad \text{where} \quad \sigma_w(f^n_0) = -\left(\sum_l v_l^- f^n_{0,l}\omega_l\right) / \left(\sum_l v_l^+ \mathcal{M}_l[1, \mathbf{u}_w, T_w]\omega_l\right).$$

It can easily seen that this definition ensures the mass conservation. Indeed, the mass flux across the wall is

$$\begin{aligned}
\sum_k \mathcal{F}^n_{1/2,k}\omega_k &= \sum_k \left(v_k^+ f^n_{0,k} + v_k^- f^n_{1,k}\right)\omega_k \\
&= \sum_k \left(-v_k^+ \frac{\sum_l v_l^- f^n_{0,l}\omega_l}{\sum_l v_l^+ \mathcal{M}_l[1,\mathbf{u}_w,T_w]\omega_l}\mathcal{M}_k[1,\mathbf{u}_w,T_w]\right)\omega_k + \sum_k \left(v_k^- f^n_{1,k}\right)\omega_k \\
&= -\sum_l \left(v_l^- f^n_{0,l}\right)\omega_l + \sum_k \left(v_k^- f^n_{1,k}\right)\omega_k \\
&= 0,
\end{aligned}$$

since $f^n_{0,k} = f^n_{1,k}$ for $v_k < 0$.

3.1.2 Second order finite volume scheme with flux limiters

In this kind of scheme, a nonlinear limitation is applied to a centered numerical flux (which is second order accurate) to ensure a stability property. Here, we use the Yee limiter, which ensures that the scheme is "Total Variation Diminishing" (TVD) (see [23]):

$$\begin{cases}
\mathcal{F}^n_{i+\frac{1}{2},k} = v_k^+ f^n_{i,k} + v_k^- f^n_{i+1,k} + |v_k|\dfrac{1}{2}\Phi^n_{i+1/2,k}, \\
\Phi^n_{i+1/2,k} = \mathrm{minmod}\Big(\Delta f^n_{i-1/2,k}, \Delta f^n_{i+1/2,k}, \Delta f^n_{i+3/2,k}\Big), \\
\Delta f^n_{i+1/2,k} = f^n_{i+1,k} - f^n_{i,k}.
\end{cases} \tag{16}$$

where the minmod function is defined by

$$\mathrm{minmod}(x,y,z) = \begin{cases} \mathrm{sgn}(x)\ \min(|x|,|y|,|z|) & \text{if } \mathrm{sgn}(x) = \mathrm{sgn}(y) = \mathrm{sgn}(z), \\ 0 \text{ in other cases.} \end{cases}$$

Like in the first order scheme, some ghost cell values have to be defined to compute the numerical flux at the wall interface $\mathcal{F}^n_{\frac{1}{2},k}$. Indeed, the first order part of the flux requires the value of $f^n_{0,k}$ for incoming velocities ($v_k > 0$), while the limiter needs $f^n_{0,k}$ and $f^n_{-1,k}$ for every velocities. Again, these ghost cell values have to be defined so as to account for the boundary condition (13)–(14) to satisfy a zero mass flux across the wall.

A simple idea that satisfies these constraints is the following. For outgoing velocities, we define $f^n_{0,k}$ and $f^n_{-1,k}$ by a zeroth order extrapolation from the first boundary cell:

$$f^n_{-1,k} = f^n_{0,k} = f^n_{1,k}.$$

For incoming velocities, we define $f^n_{0,k}$ like in the first order scheme, that is to say:

$$f^n_{0,k} = \sigma_w(f^n_{0,k})\mathcal{M}_k, \qquad \text{where} \qquad \sigma_w(f^n_{0,k}) = -\left(\sum_l v_l^- f^n_{0,l}\omega_l\right)\left(\sum_l v_l^+ \mathcal{M}_l\omega_l\right)^{-1}.$$

And again, $f^n_{-1,k}$ is defined by zeroth order extrapolation with $f^n_{-1,k} = f^n_{0,k}$.

This definition implies that the numerical flux at the wall interface $\mathcal{F}^n_{\frac{1}{2},k}$ reduces to the first order flux $v^+_k f^n_{0,k} + v^-_k f^n_{1,k}$, since $\Delta f^n_{-\frac{1}{2},k} = f^n_{0,k} - f^n_{-1,k} = 0$ by construction, and hence the limiter $\Phi^n_{1/2,k}$ is zero. Consequently, the mass conservation is satisfied (see section 3.1.1). At the same time, the drawback of this approach is that the numerical flux at the wall is only first order accurate, while it is second order inside the computational domain. This lower accuracy at the wall can be clearly observed in our numerical tests (see section 4).

To increase the accuracy of the scheme, a natural idea is to use a first order extrapolation to define $f^n_{0,k}$ and $f^n_{-1,k}$ for outgoing velocities, and then to use the boundary conditions to define these values for incoming velocities. This might give a second order flux, but we have not been able to find a definition for which the conservation property still holds. In our opinion, it is unlikely that such a definition exist (see an explanation at the end of section 3.1.3).

Consequently, we believe that such a scheme cannot be at the same time second order up to the boundary and conservative. This is why we propose to consider another kind of second order scheme in the following section.

3.1.3 Second order finite volume second order scheme based on linear reconstruction

In the finite volume schemes using a linear reconstruction, the numerical fluxes appearing in relation (15) are still defined as upwind fluxes, but with new values at the cells interfaces, obtained with a linear reconstruction of the distribution f_k inside each cell [14]:

$$\begin{cases} \mathcal{F}^n_{i+\frac{1}{2},k} = v^+_k f^{n,-}_{i+\frac{1}{2},k} + v^-_k f^{n,+}_{i+\frac{1}{2},k}, \\ f^{n,-}_{i+\frac{1}{2},k} = f^n_{i,k} + \dfrac{\Delta x_i}{2}\delta^n_{i,k}, \\ f^{n,+}_{i+\frac{1}{2},k} = f^n_{i+1,k} - \dfrac{\Delta x_{i+1}}{2}\delta^n_{i+1,k}, \end{cases} \tag{17}$$

where $\delta^n_{i,k}$ is the slope of the linear reconstruction of f in cell i. The most classical way to compute this slope is a least square method, which gives, for a regular mesh, the centered slope

$$\delta^n_{i,k} = \frac{f^n_{i+1,k} - f^n_{i-1,k}}{2\Delta x_i}. \tag{18}$$

To obtain a TVD scheme, the slope must be limited to avoid the creation of new extrema. Here, we use the MC slope limiter defined on each cell by

$$\delta^{n,lim}_{i,k} = \text{minmod}\left(\delta^n_{i,k}, 2\alpha_i \frac{f^n_{i,k} - f^n_{i-1,k}}{\Delta x_i}, 2\alpha_i \frac{f^n_{i+1,k} - f^n_{i,k}}{\Delta x_i}\right), \tag{19}$$

where α_i is a free parameter between 0 and 1 [14].

When this scheme is applied to the first cell $i = 1$, the numerical flux $\mathcal{F}^n_{\frac{1}{2},k}$ is

$$\mathcal{F}^n_{\frac{1}{2},k} = v_k^+ f^{n,-}_{\frac{1}{2},k} + v_k^- f^{n,+}_{\frac{1}{2},k}.$$

It uses two values of the distribution at the solid interface: $f^{n,+}_{\frac{1}{2},k}$ is the value on the right side of the wall, required for outgoing velocities $v_k < 0$, given by the linear reconstruction

$$f^{n,+}_{\frac{1}{2},k} = f^n_{1,k} - \frac{\Delta x_1}{2}\delta^{n,lim}_{1,k}, \tag{20}$$

while $f^{n,-}_{\frac{1}{2},k}$ is the value on the left side of the wall, required for incoming velocities $v_k > 0$, given by the linear reconstruction

$$f^{n,-}_{\frac{1}{2},k} = f^n_{0,k} + \frac{\Delta x_0}{2}\delta^{n,lim}_{0,k}, \tag{21}$$

where the slopes are defined by (18)–(19) with $i = 1$ and $i = 0$, respectively. This requires to define two ghost cell values $f^n_{0,k}$ and $f^n_{-1,k}$, and the corresponding cell size Δx_0. Again, they have to be defined so as to account for the boundary condition and to preserve the conservation property.

First, note that for the conservation property holds, it is sufficient that the value of f at the wall interface satisfies

$$f^{n,-}_{\frac{1}{2},k} = \sigma_w(f^{n,+}_{\frac{1}{2},k})\mathcal{M}_k. \tag{22}$$

Consequently, we have to construct the ghost cell values so that relations (20)–(22) hold. This can be done as follows.

The method, inspired by [11, 8], consists in first defining the wall interface values $f^{n,\pm}_{\frac{1}{2},k}$ by extrapolation (for outgoing velocities) and by the boundary condition (for incoming velocities), and then in defining the ghost cell values $f^n_{0,k}$ and $f^n_{-1,k}$ so that (20)–(21) hold. This method is detailed below in three steps, and summarized in figure 1. Note that in the following, we will assume that the ghost cells have the same size as the first cell: $\Delta x_{-1} = \Delta x_0 = \Delta x_1$.

• Step 1: computation of $f^{n,+}_{1/2,k}$ for outgoing velocities $v_k < 0$.
This value is defined by a linear extrapolation using the values $f^n_{1,k}$ and $f^n_{2,k}$:

$$f^{n,+}_{1/2,k} = \frac{3}{2}f^n_{1,k} - \frac{1}{2}f^n_{2,k}. \tag{23}$$

• Step 2: computation of $f^{n,-}_{1/2,k}$ for incoming velocities $v_k > 0$.
We use the boundary condition (13)–(14) to get

$$f^{n,-}_{1/2,k} = \sigma_w(f^{n,+}_{1/2})\mathcal{M}^n_k. \tag{24}$$

• Step 3: definition of the values $f^n_{0,k}$ and $f^n_{-1,k}$ in the ghost cells.

For outgoing velocities, only the value of $f^n_{0,k}$ is required. We use the same linear extrapolation as used to compute extrapolation $f^{n,+}_{1/2,k}$ (see Step 1) to get

$$f^n_{0,k} = 2f^n_{1,k} - f^n_{2,k}.$$

For incoming velocities, we need the values of $f^n_{0,k}$ and $f^n_{-1,k}$. Then we use again a linear extrapolation, but based on the values of the incoming value of the wall interface distribution $f^{n,-}_{1/2,k}$ and on $f^n_{1,k}$. This gives

$$\begin{aligned} f^n_{0,k} &= 2f^{n,-}_{1/2,k} - f^n_{1,k}, \\ f^n_{-1,k} &= 4f^{n,-}_{1/2,k} - 3f^n_{1,k}. \end{aligned}$$

Now it is not difficult to prove that these definitions satisfy the previous constraints, provided that $\alpha_i \geq \frac{1}{2}$. First, (22) is imposed at step 2, and hence it is satisfied, which gives mass conservation. Now, it remains to prove that $f^{n,\pm}_{\frac{1}{2},k}$ defined by (23) and (24) also satisfy (20) and (21). This is due to the extrapolation procedures that make the points $(x_i, f^n_{i,k})$ are on the same straight line, and hence the limiters can be computed. Indeed, for instance, we have for incoming velocities $v_k > 0$:

$$\begin{aligned} \delta^{n,lim}_{0,k} &= \text{minmod}\left(\frac{f^n_{1,k} - f^n_{-1,k}}{2\Delta x_0}, 2\alpha_0\frac{f^n_{0,k} - f^n_{-1,k}}{\Delta x_0}, 2\alpha_0\frac{f^n_{1,k} - f^n_{0,k}}{\Delta x_0}\right) \\ &= \text{minmod}\left(2\frac{f^n_{1,k} - f^{n,-}_{1/2,k}}{\Delta x_0}, (2\alpha_0)2\frac{f^n_{1,k} - f^{n,-}_{1/2,k}}{\Delta x_0}, (2\alpha_0)2\frac{f^n_{1,k} - f^{n,-}_{1/2,k}}{\Delta x_0}\right) \\ &= 2\frac{f^n_{1,k} - f^{n,-}_{1/2,k}}{\Delta x_0}. \end{aligned}$$

Consequently, the right-hand side of (21) is

$$\begin{aligned} f^n_{0,k} + \frac{\Delta x_0}{2}\delta^{n,lim}_{0,k} &= 2f^{n,-}_{1/2,k} - f^n_{1,k} + f^n_{1,k} - f^{n,-}_{1/2,k} \\ &= f^{n,-}_{1/2,k} \end{aligned}$$

and (21) is satisfied. For outgoing velocities, we have

$$\begin{aligned} \delta^{n,lim}_{1,k} &= \text{minmod}\left(\frac{f^n_{2,k} - f^n_{0,k}}{2\Delta x_1}, 2\alpha_1\frac{f^n_{1,k} - f^n_{0,k}}{\Delta x_1}, 2\alpha_1\frac{f^n_{2,k} - f^n_{1,k}}{\Delta x_1}\right) \\ &= \text{minmod}\left(\frac{f^n_{2,k} - f^n_{1,k}}{\Delta x_1}, 2\alpha_1\frac{f^n_{2,k} - f^n_{1,k}}{\Delta x_1}, 2\alpha_1\frac{f^n_{2,k} - f^n_{1,k}}{\Delta x_1}\right) \\ &= \frac{f^n_{2,k} - f^n_{1,k}}{\Delta x_1}. \end{aligned}$$

Consequently, the right-hand side of (20) is

$$\begin{aligned} f_{1,k}^n - \frac{\Delta x_1}{2}\delta_{1,k}^{n,lim} &= \frac{3}{2}f_{1,k}^n - \frac{1}{2}f_{2,k}^n \\ &= f_{1/2,k}^{n,+} \end{aligned}$$

from (23), and hence (20) is satisfied.

In summary, we have proved that this finite volume scheme is based on slope limiters whose ghost cell values are consistent with the slope reconstruction up to the solid boundary: this implies the second order accuracy up to the boundary. Moreover, we have proved that this scheme also preserves the mass conservation even with solid boundaries. Finally, note that even if the extrapolation procedure we use at the solid wall might induce non positive values of the distribution functions, we did not observe this problem in our numerical tests. This is probably due to the fact that we use small cells in the Knudsen layer, which make the gradients, and hence the slopes, small enough too avoid the creation of negative values.

Remark 3.1. The fact that scheme with a flux limiter presented in section 3.1.2 cannot be both second order and conservative at the solid wall can be seen as follows.

The previous analysis for the scheme with a slope limiter relies on the fact that the minmod function (19) reduces to a single slope. Consequently, the scheme is linear at the solid wall, and hence is compatible with boundary condition (22) (which is linear too). This implies the conservation property. This reduction is due to the fact that the ghost cell values $f_{0,k}$ and $f_{-1,k}$ are defined by extrapolations that make all the points used in (19) *aligned* (and hence with three equal slopes).

For the scheme with a flux limiter, this extrapolation cannot make all the points aligned. Indeed, the limiter (16) uses the same stencil for negative and positive velocities (it is a "symmetric" limiter (see [23]). This implies that for positive velocities, $f_{-1,k}^n$ and $f_{0,k}^n$ are defined through extrapolation of $f_{\frac{1}{2},k}^{-,n}$ and $f_{1,k}^n$, but they cannot be aligned with $f_{2,k}^n$, in general (see figure 2). Our previous analysis cannot be applied, and there is no reason for the conservation property holds true.

However, if instead a non symmetric (or "upwind") flux limiter is used (see [14]), it is still possible to prove the conservation property. Such is scheme is not used in this paper.

3.2 Discontinuous Galerkin scheme

In finite volume methods, the distribution is approximated by a piecewise constant function (on each cell, the discrete distribution is equal to its cell average). Discontinuous Galerkin schemes can be viewed as an extension of the finite volume method in which the distribution is now approximated by piecewise polynomial functions. Here, we will consider a piecewise linear approximation.

3.2.1 Weak form and piecewise linear approximation

On each cell $\Omega_i = [x_{i-\frac{1}{2}}, x_{i+\frac{1}{2}}]$, we use two basis affine functions $\varphi_{i,1}$ and $\varphi_{i,2}$ such that $\varphi_{i,1}(x_{i-\frac{1}{2}}) = 1$, $\varphi_{i,1}(x_{i+\frac{1}{2}}) = 0$, and $\varphi_{i,2}(x_{i-\frac{1}{2}}) = 0$, $\varphi_{i,2}(x_{i+\frac{1}{2}}) = 1$. We project equation (8) in this basis and integrate by parts to get for every i and $p = 1, 2$:

$$\int_{\Omega_i} \frac{\partial f_k}{\partial t}(t,x)\varphi_{i,p}(x)\,dx - \int_{\Omega_i} v_k f_k(t,x)\partial_x\varphi_{i,p}(x)\,dx$$
$$+ \Big(v_k f_k(t, x_{i+\frac{1}{2}})\varphi_{i,p}(x_{i+\frac{1}{2}}) - v_k f_k(t, x_{i-\frac{1}{2}})\varphi_{i,p}(x_{i-\frac{1}{2}})\Big) = \int_{\Omega_i} \frac{1}{\tau_i}\left(\mathcal{M}_k[\rho, \mathbf{u}, T] - f_k\right)\varphi_{i,p}(x)\,dx, \tag{25}$$

Now, we assume that $f_k(t,x)$ can be approximated on each cell by a piecewise linear function $\hat{f}_k(t,x)$ defined by $\hat{f}_k(t,x)|_{\Omega_i} = f_{i,k}(t,x) = f_{i,k,1}(t)\varphi_{i,1}(x) + f_{i,k,2}(t)\varphi_{i,2}(x)$ (see figure 3). Note that while the components $f_{i,k,1}$ and $f_{i,k,2}$ are also the pointwise values of $f_{i,k}$ at the edges of Ω_i, the whole function $\hat{f}_k$ itself is not continuous across these edges: indeed, at each cell edge $x_{i+\frac{1}{2}}$, $\hat{f}_k$ has two left and right values $f_{i,k}(t, x_{i+\frac{1}{2}}) = f_{i,k,2}$ and $f_{i+1,k}(t, x_{x_{i+\frac{1}{2}}}) = f_{i+1,k,1}$ (see figure 3).

This approximation has now to be injected in the weak form (25). The first term of the left-hand side is easily computed

$$\sum_{q=1}^{2} \int_{\Omega_i} \frac{\partial f_{i,k,q}}{\partial t}\varphi_{i,q}(x)\varphi_{i,p}(x)\,dx = \sum_{q=1}^{2} m^i_{pq}\frac{\partial f_{i,k,q}}{\partial t}, \tag{26}$$

where the (m^i_{pq}) form the 2×2 matrix

$$(m^i_{pq}) = \bar{\bar{M}}_i = \frac{|\Omega_i|}{6}\begin{pmatrix} 2 & 1 \\ 1 & 2 \end{pmatrix}. \tag{27}$$

The second term of the left-hand side is

$$-v_k \int_{\Omega_i} f_{i,k}(x)\frac{\partial \varphi_{i,p}(x)}{\partial x}\,dx = \sum_{q=1}^{2} d_{pq} f_{i,k,q}, \tag{28}$$

where the (d_{pq}) form the 2×2 matrix

$$(d_{pq}) = \bar{\bar{D}}_k = \frac{v_k}{2}\begin{pmatrix} 1 & 1 \\ -1 & -1 \end{pmatrix}. \tag{29}$$

For the third term of the left-hand side of (25), we muse take into account that the piecewise linear approximation of f_k is not continuous across cell edges (see the remark above). Consequently, we write this term as $v_k\hat{f}_k(t, x_{i+\frac{1}{2}})\varphi_{i,p}(x_{i+\frac{1}{2}}) - v_k\hat{f}_k(t, x_{i-\frac{1}{2}})\varphi_{i,p}(x_{i-\frac{1}{2}})$,

where a single value for $\hat{f}_k(t, x_{i+\frac{1}{2}})$ has to be defined. A good choice (for accuracy, stability, and treatment of boundary conditions) is to use the upwind value

$$\hat{f}_k(t, x_{i+\frac{1}{2}}) = \begin{cases} f_{i,k,2}(t) & \text{if } v_k > 0, \\ f_{i+1,k,1}(t) & \text{if } v_k < 0. \end{cases}$$

Taking into account that the basis functions $\varphi_{i,p}$ take values 0 or 1 at the cell edges of Ω_i, we get

$$v_k \hat{f}_k(t, x_{i+\frac{1}{2}})\varphi_{i,p}(x_{i+\frac{1}{2}}) - v_k \hat{f}_k(t, x_{i-\frac{1}{2}})\varphi_{i,p}(x_{i-\frac{1}{2}}) = \begin{cases} -v_k^+ f_{i-1,k,2}(t) - v_k^- f_{i,k,1}(t) & \text{for } p = 1, \\ v_k^+ f_{i,k,2}(t) + v_k^- f_{i+1,k,1}(t) & \text{for } p = 2. \end{cases} \tag{30}$$

The right-hand side of (25) is obtained by using the same piecewise linear approximation for each term, which gives

$$\int_{C_i} \frac{1}{\tau}(\mathcal{M}_k[\hat{\mathbf{U}}] - \hat{f}_k)\varphi_{i,p}(x)\, dx = \sum_{q=1}^{2} m_{pq}^i \frac{1}{\tau_{i,q}} \left(\mathcal{M}_{i,k,q} - f_{i,k,q}\right), \tag{31}$$

where m_{pq}^i has been defined in (27), $\mathcal{M}_{i,k,q} = \mathcal{M}_k[\rho_{i,q}, \mathbf{u}_{i,q}, T_{i,q}]$, $\tau_{i,q} = \tau(\rho_{i,q}, T_{i,q})$, and the macroscopic quantities $\rho_{i,q}, \mathbf{u}_{i,q}, T_{i,q}$ are defined by applying (9) in each cell.

Finally, we collect the different terms (26–31), and we find that the approximation of (25) can be written in the following vectorial form

$$\bar{\bar{M}}_i \frac{\partial \mathbf{f}_{i,k}}{\partial t} + \bar{\bar{D}}_k\, \mathbf{f}_{i,k} + \left(\bar{\bar{A}}_k\, \mathbf{f}_{i-1,k} + \bar{\bar{B}}_k\, \mathbf{f}_{i,k} + \bar{\bar{C}}_k\, \mathbf{f}_{i+1,k}\right) = \bar{\bar{M}}_i \frac{1}{\boldsymbol{\tau}_i}(\boldsymbol{\mathcal{M}}_{i,k} - \mathbf{f}_{i,k}), \tag{32}$$

where we use the following notations for the two-component vectors $\mathbf{f}_{i,k} = (f_{i,k,1}, f_{i,k,2})^T$ and $\boldsymbol{\mathcal{M}}_{i,k} = (\mathcal{M}_{i,k,1}, \mathcal{M}_{i,k,2})^T$, the 2×2 matrices $\bar{\bar{A}}_k = \left(\begin{smallmatrix} 0 & -v_k^+ \\ 0 & 0 \end{smallmatrix}\right)$, $\bar{\bar{B}}_k = \left(\begin{smallmatrix} -v_k^- & 0 \\ 0 & v_k^+ \end{smallmatrix}\right)$, $\bar{\bar{C}}_k = \left(\begin{smallmatrix} 0 & 0 \\ v_k^- & 0 \end{smallmatrix}\right)$, while the matrices $\bar{\bar{M}}_i$ and $\bar{\bar{D}}_k$ have been defined in (27) and (29). Note that the product of vectors $\frac{1}{\boldsymbol{\tau}_i}(\boldsymbol{\mathcal{M}}_{i,k} - \mathbf{f}_{i,k})$ must be understood component-wise. Multiplying (32) by the matrix $\bar{\bar{M}}_i^{-1} = \frac{2}{|\Omega_i|}\left(\begin{smallmatrix} 2 & -1 \\ -1 & 2 \end{smallmatrix}\right)$ (the inverse of $\bar{\bar{M}}_i$), we obtain the semi-discrete scheme

$$\begin{aligned} \frac{\partial \mathbf{f}_{i,k}}{\partial t} = &- \frac{1}{|\Omega_i|}\begin{pmatrix} 3v_k & 3v_k \\ -3v_k & -3v_k \end{pmatrix}\mathbf{f}_{i,k} \\ &- \frac{2}{|\Omega_i|}\left[\begin{pmatrix} 0 & -2v_k^+ \\ 0 & v_k^+ \end{pmatrix}\mathbf{f}_{i-1,k} + \begin{pmatrix} -2v_k^- & -v_k^+ \\ v_k^- & 2v_k^+ \end{pmatrix}\mathbf{f}_{i,k} + \begin{pmatrix} -v_k^- & 0 \\ 2v_k^- & 0 \end{pmatrix}\mathbf{f}_{i+1,k}\right] \\ &+ \frac{1}{\boldsymbol{\tau}_i}(\boldsymbol{\mathcal{M}}_{i,k} - \mathbf{f}_{i,k}). \end{aligned} \tag{33}$$

3.2.2 Time discretization

As shown in [7], Discontinuous Galerkin scheme are unstable when used with a forward Euler method. Since we are interested in steady flows only, we use the same linearized implicit scheme as for the finite volume method (see [15, 1]).

3.2.3 Boundary conditions

The Discontinuous Galerkin scheme is very compact, as the value $\mathbf{f}_{i,k}^{n+1}$ only depends on $\mathbf{f}_{i,k}^n$, $f_{i-1,k,2}^n$ and $f_{i+1,k,1}^n$. We just need one rank of ghost cells on each boundary. Moreover, the value of f_k^n in the ghost cell has just to be defined on the side corresponding to the interface between the wall and the gas, this means $f_{0,k,2}^n$ for the left boundary (and $f_{i_{max}+1,k,1}^n$ at the right one).

For the left wall, we use a technique which is close to what is done with the finite volume scheme (except that we do not need extrapolation here): we define the distribution at the wall by

$$f_{wall,k}^n = \begin{cases} f_{1,k,1}^n & \text{for } v_k < 0, \\ f_{0,k,2}^n & \text{for } v_k > 0, \end{cases}$$

see figure 3. The ghost cell value $f_{0,k,2}^n$ is defined by applying the boundary condition (13)–(14) to $f_{wall,k}^n$ to get for $v_k > 0$

$$f_{0,k,2} = \sigma_1^n \, \mathcal{M}_k[1, u_w, T_w],$$

where $\sigma_1^n = -\left(\sum_k v_k^- f_{1,k,1}^n \omega_k\right) / \left(\sum_k v_k^+ \mathcal{M}_k^n[1, u_w, T_w]\omega_k\right)$.

4 Numerical results

4.1 Test-case and reduced model in 1D: Couette flow

We consider a plane Couette flow of argon: the gas lies between two flat walls, both walls are at the same temperature T_w, the left wall is at rest, while the right wall moves upward with the velocity $\mathbf{u_w} = (0, u_w, 0)^T$. The resulting flow is one dimensional. With the standard reduced distribution technique [6], the 3D BGK equation (4) reduces to the following system of 3 kinetic equations

$$\partial_t \begin{pmatrix} F \\ G \\ H \end{pmatrix} + v_x \partial_x \begin{pmatrix} F \\ G \\ H \end{pmatrix} = \frac{1}{\tau} \begin{pmatrix} \mathcal{M}[\rho, \mathbf{u}, \mathbf{T}] - \mathbf{F} \\ \mathcal{N}[\rho, \mathbf{u}, \mathbf{T}] - \mathbf{G} \\ \mathcal{P}[\rho, \mathbf{u}, \mathbf{T}] - \mathbf{H} \end{pmatrix},$$

where the reduced distributions are

$$\begin{pmatrix} F \\ G \\ H \end{pmatrix} = \int_{\mathbb{R}^2} \begin{pmatrix} 1 \\ \frac{1}{2}(v_x^2 + v_y^2) \\ v_z \end{pmatrix} f \, dv_x dv_y,$$

the macroscopic quantities mass density, velocity, temperature, and normal heat flux, are

$$\begin{pmatrix} \rho \\ \rho u_x \\ \rho u_y \\ \frac{3}{2}\rho R T \end{pmatrix} = \int_{\mathbb{R}^2} \begin{pmatrix} F \\ v_x F \\ H \\ \frac{1}{2}(v_x - u_x)^2 F + G \end{pmatrix} dv_x,$$

and

$$q_x = \int_{\mathbb{R}^2} \frac{1}{2}(v_x - u_x)^3 F + (v_x - u_x)(G - u_y H)\, dv_x,$$

and the reduced Maxwellians are

$$\mathcal{M}[\rho, \mathbf{u}, T] := \frac{\rho}{\sqrt{2\pi RT}} \exp\left(-\frac{|v_x - u_x|^2}{2RT}\right),$$

$$\mathcal{N}[\rho, \mathbf{u}, T] := \left(RT + \frac{u_y^2}{2}\right) \mathcal{M}[\rho, \mathbf{u}, T], \quad \text{and} \quad \mathcal{P}[\rho, \mathbf{u}, T] := u_y\, \mathcal{M}[\rho, \mathbf{u}, T].$$

The diffuse reflection boundary condition (6)–(7) reduces to

$$\begin{pmatrix} F \\ G \\ H \end{pmatrix}|_{\text{wall, } \mathbf{v}\cdot\mathbf{n}>0} = \sigma_w(F) \begin{pmatrix} \mathcal{M}[1, \mathbf{u}_w, T_w] \\ \mathcal{N}[1, \mathbf{u}_w, T_w] \\ \mathcal{P}[1, \mathbf{u}_w, T_w] \end{pmatrix},$$

where $\sigma_w(F) = -\left(\int_{v_x n(x)<0} v_x F(t, \mathbf{x}, v_x)\, dv_x\right) \left(\int_{v_x n(x)>0} v_x \mathcal{M}[1, \boldsymbol{u}_w, T](v_x)\, dv_x\right)^{-1}$, with $n(x) = 1$ at the left wall and $n(x) = -1$ at the right wall.

All the schemes described in the previous section readily apply to this system.

4.2 Comparison of second order Finite Volume schemes on the 1D Couette flow

The flow parameters and gas properties are given in Table 2. The Knudsen number is based on the distance between the plates, and the mean free path is defined by (see Bird [3], with the tables for the values of μ_0, T_0 and ω)

$$\lambda = \left[\sqrt{2}\pi d^2 \frac{\rho}{m} \left(\frac{T_0}{T}\right)^{\omega - \frac{1}{2}}\right]^{-1} \quad \text{with} \quad d = \left[\frac{5(\alpha+1)(\alpha+2)\sqrt{\pi^{-1} m k_b T}}{4\alpha(5-2\omega)(7-2\omega)\mu_0}\right]^{\frac{1}{2}}$$

where k_b is the Boltzmann constant and m the molecular mass of the gas.

For this problem, we use a uniform mesh of 100 cells. The discrete velocity grid is a uniform grid of 40 points with bounds ± 953 m.s^{-1}. We compare here four schemes:

- the second order finite volume scheme with the Yee flux limiter (16) and first order boundary conditions, as described in section 3.1.2, and denoted here by "O2-flux";
- the second order finite volume scheme using linear reconstruction (17), with second order boundary conditions (20) and (21), without limiter (i.e. with slope (18)), denoted by "O2-slope-nolim";
- the same scheme but with limited slope (19) with $\alpha_i = 1/2$, denoted by "O2-slope";

- the same scheme but with boundary conditions of first order only, denoted by "O2-slope-BC-O1" (that is to say with distributions at the wall defined by (20) and (21) with zero limited slopes).

We show on Figure 4 the heat flux and the horizontal velocity obtained with these four schemes. Note that the horizontal velocity is a good indicator of accuracy, since its exact value is zero in the whole domain. We can see that the schemes with first order boundary conditions (O2-flux and O2-slope-BC-O1) have a very bad behavior in the near-wall zone, where we observe a strong variation of the velocity and the heat flux, while the two other second order schemes give a correct solution. This result confirms the analysis of section 3.1.2: the flux-limiter scheme degenerates into a first order scheme in the near-wall zone, and the boundary conditions have to be discretized in a way which is consistent with the second order scheme.

Note that the slope limitation does not seem to be useful here: the scheme without limitation is the most accurate, as this can be seen from the horizontal velocity profiles (its exact value is zero). However, we will see in next section that this limitation is necessary for multidimensional cases.

4.3 Validation of the Finite Volume scheme in 2D

The kinetic code of the CEA is dedicated to the simulation of hypersonic flows based on the BGK model, to make 2D plane, axisymmetric and 3D simulations of rarefied flows for monoatomic and diatomic gases. We refer to [1] for more details on this code. It uses two second order finite volume schemes on curvilinear meshes. The first one is the version with flux limiter method, as described in section 3.1.2, with first order boundary conditions. The other scheme is the one with the linear reconstruction and second order boundary conditions, as described in section 3.1.3. Since the space mesh is not uniform, formulas in section 3.1.3 (in particular (18)) have to be modified accordingly.

The test case is a steady flow of argon over a cylinder of radius 0.1 m at Mach 5, see figure 5. The density and pressure are that of the air at an altitude of 60 km. Namely, we have $\rho = 3.059\ 10^{-4}\text{kg/m}^3$, $u = 1750$ m/s and $T = 352.6$ K. The Knudsen number, based on the radius of the cylinder, is $\text{Kn} = 2.2\ 10^{-3}$, so the flow is rather dense, and a comparison with a Navier-Stokes simulation (with no-slip and no temperature jump) is relevant. With such a small Knudsen number, we can expect a difference between BGK and Navier-Stokes results lower than 1%. As an illustration, the 2D velocity and Mach number fields are shown in figure 6, with the mesh used for the simulation, made with the finite volume scheme with slope limiters.

We compute the normal component of the heat flux along the boundary of the cylinder and compare the following finite volume schemes:

- first order scheme (O1);
- second order scheme with Yee flux limiters with first order boundary conditions (O2-flux)

- second order scheme with slope limiters and second order boundary conditions (O2-slope);
- Navier-stokes solution (NS), obtained with a finite volume code of the CEA.

In figure 7, we show a comparison of the normal component of the heat flux along the solid boundary obtained with these schemes on different meshes (from 25×50 to 25×200 cells), with an increasing number of cells in the direction orthogonal to the solid boundary. Like in the 1D Couette flow, we observe that the second order scheme with flux limiter is not sufficient to compute accurately the heat flux, while the second order scheme with linear reconstruction, slope limiters, and second order boundary conditions, is much more accurate. Note that for this test case, this last scheme requires a real limitation: the coefficient α_i of the MC limiter (19) has been taken equal to 0.75. Indeed, the code produces too strong oscillations for larger values: this induces negative density and temperature that make the code stop.

4.4 Comparison between the Discontinuous Galerkin and Finite Volume schemes

We compare the Discontinuous Galerkin scheme presented in section 3.2 to the finite volume schemes presented in section 3.1 and already analyzed in the numerical comparisons above.

The test case is the same Couette flow as in section 4.2. We use uniform meshes with 12, 100, 800 and 6400 cells. We present on Figure 8 the horizontal velocity (which should be exactly zero) and the heat flux obtained for each scheme on each mesh. We can observe that the Discontinuous Galerkin scheme is very close to the second-order finite volume one; the results are far more accurate than with the first-order finite volume scheme (note that the second order scheme with flux limiters is not shown here).

With those results, we can compute the convergence rate of each scheme, given in Table 1 for the temperature and the heat flux, in the L^2 norm. The convergence rates are consistent

	q_x	T
O1	0.98	1.06
O2-slope	1.89	1.96
O2-flux	1.44	1.84
DG	1.74	1.64

Table 1: 1D Couette flow: convergence orders in L^2 norm for the first order upwind finite volume scheme (O1), second order finite volume scheme with slope limiters (O2-slope), finite volume scheme with flux limiters (O2-flux), discontinuous Galerkin scheme (DG).

with our analysis and with the theory. The upwind finite volume scheme shows a first order

convergence rate, the finite volume scheme with slope limiters shows an almost second order convergence rate, the discontinuous Galerkin scheme with upwind fluxes shows an almost 3/2 order convergence rate (see [12]), while, as expected, the finite volume scheme with flux limiters has an order of convergence smaller than 2.

The corresponding error curves for the heat flux are given in Figure 9. It can be seen that the finite volume scheme with flux limiters is not very accurate: even the first order scheme is more accurate, while the numerical boundary flux is the same for both schemes. This is probably due to the inconsistency between the treatment of inner and boundary cells with these flux limiters. The other schemes are much more accurate, and very close, even if the discontinuous Galerkin scheme is a bit more accurate than the finite volume scheme with slope limiters.

5 Conclusions and perspectives

We have studied two different second order finite volume schemes applied to a kinetic equation (the BGK model of kinetic gas theory). We have shown that a scheme with a nonlinear symetric flux limiter is not second order accurate up to a solid boundary in case of diffuse reflection conditions, which strongly decreases its accuracy. At the contrary, the technique of slope limiters allows to reach second order accuracy up to the boundary. The scheme with slope limiters has been applied to a 2D supersonic problem with a curvilinear mesh, on which it shows a much higher accuracy to compute the heat flux along the wall (as compared to the scheme with flux limiters), which is of paramount importance in aerodynamics.

Moreover, the finite volume schemes have been compared to an upwind Discontinuous Galerkin method (with piecewise linear elements). This scheme does not require any specific treatment at the solid wall, and the boundary condition can be directly applied to compute the flux at the gas/solid interface. The accuracy of this scheme is the same as the finite volume scheme with slope limiters. However, the Discontinuous Galerkin scheme requires twice as degrees of freedom as the finite volume scheme. Further work would be necessary to compare the performance of these schemes on 2D curvilinear meshes.

References

[1] C. Baranger, J. Claudel, N. Hérouard, and L. Mieussens. Locally refined discrete velocity grids for stationary rarefied flow simulations. *Journal of Computational Physics*, 257, Part A(0):572 – 593, 2014.

[2] P.L. Bhatnagar, E.P. Gross, and M. Krook. A model for collision processes in gases. I. small amplitude processes in charged and neutral one-component systems. *Phys. Rev.*, 94:511–525, 1954.

[3] G.A. Bird. *Molecular Gas Dynamics and the Direct Simulation of Gas Flows*. Oxford Science Publications, 1994.

[4] C. Cercignani. *The Boltzmann Equation and Its Applications*, volume 68. Springer-Verlag, Lectures Series in Mathematics, 1988.

[5] Yingda Cheng, I.M. Gamba, A. Majorana, and C-W Shu. Discontinuous galerkin methods for the boltzmann-poisson systems in semiconductor device simulations. In *27th International Symposium on Rarefied Gas Dynamics*, volume 1333 of *AIP Conference Proceedings*, pages 890–895, 2011.

[6] C. K. Chu. Kinetic-theoretic description of the formation of a shock wave. *Physics of Fluids (1958-1988)*, 8(1):12–22, 1965.

[7] Bernardo Cockburn and Chi-Wang Shu. Runge–Kutta Discontinuous Galerkin methods for convection-dominated problems. *Journal of Scientific Computing*, 16(3):173–261, 2001.

[8] G. Dechristé. *Méthodes numériques sur grilles cartésiennes pour le modèle BGK de l'équation de Boltzmann*. PhD thesis, Université de Bordeaux, 2014. in french.

[9] G. Dechristé and L. Mieussens. A cartesian cut cell method for rarefied flow simulations around moving obstacles. *Journal of Computational Physics*, 314:465 – 488, 2016.

[10] B. Dubroca and L. Mieussens. A conservative and entropic discrete-velocity model for rarefied polyatomic gases. In *CEMRACS 1999 (Orsay)*, volume 10 of *ESAIM Proc.*, pages 127–139 (electronic). Soc. Math. Appl. Indust., Paris, 1999.

[11] Francis Filbet and Chang Yang. An inverse Lax–Wendroff method for boundary conditions applied to Boltzmann type models. *Journal of Computational Physics*, 245(0):43 – 61, 2013.

[12] C. Johnson and J. Pitkäranta. An analysis of the discontinuous Galerkin method for a scalar hyperbolic equation. *Math. Comp.*, 46(173):1–26, 1986.

[13] Randall J. LeVeque. *Numerical methods for conservation laws*. Lectures in Mathematics ETH Zürich. Birkhäuser Verlag, Basel, 1990.

[14] Randall J. LeVeque. *Finite volume methods for hyperbolic problems*. Cambridge Texts in Applied Mathematics. Cambridge University Press, Cambridge, 2002.

[15] L. Mieussens. Discrete-velocity models and numerical schemes for the Boltzmann-BGK equation in plane and axisymmetric geometries. *J. Comput. Phys.*, 162:429–466, 2000.

[16] Luc Mieussens. *Modèles à vitesses discrètes et méthodes numériques pour l'équation de Boltzmann-BGK*. PhD thesis, Université Bordeaux 1, 1999.

[17] Luc Mieussens. Convergence of a discrete-velocity model for the Boltzmann-BGK equation. *Computers and Mathematics with Applications*, 41(1–2):83 – 96, 2001.

[18] W.H. Reed and T.R. Hill. Triangular mesh methods for the neutron transport equation. *Technical report LA-UR-73-0479*, 1973.

[19] Wei Su, Alina A. Alexeenko, and Guobiao Cai. A runge-kutta discontinuous galerkin solver for 2d boltzmann model equations: Verification and analysis of computational performance. *AIP Conference Proceedings*, 1501(1):381–388, 2012.

[20] V. A. Titarev. Efficient deterministic modelling of three-dimensional rarefied gas flows. *Communications in Computational Physics*, 12(1):162–192, 2012.

[21] P. Welander. On the temperature jump in a rarefied gas. *Arkiv für Fysik*, 7(44):507–553, 1954.

[22] K. Xu and J.-C. Huang. A unified gas-kinetic scheme for continuum and rarefied flows. *J. Comput. Phys.*, 229:7747–7764, 2010.

[23] H. C. Yee. *A Class of High-Resolution Explicit and Implicit Shock-Capturing Methods*. Von Karman Institute for Fluid Dynamics, Lectures Series, n°4. Von Karman Institute for Fluid Dynamics, 1989.

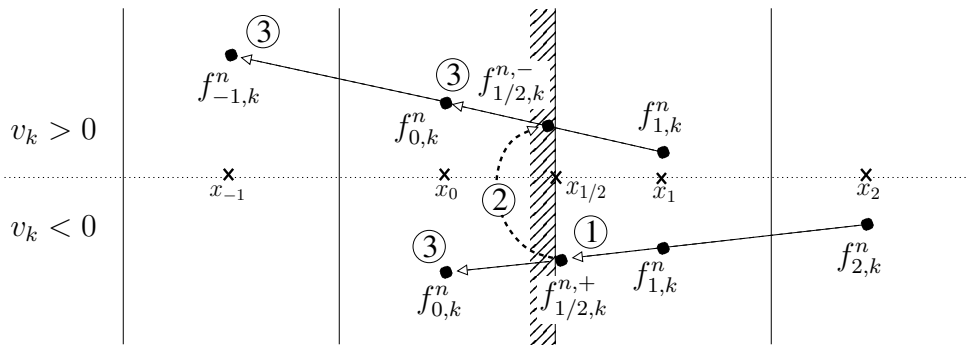

Figure 1: Finite volume scheme with a slope limiter: definition of the ghost cell values $f^n_{0,k}$ and $f^n_{-1,k}$ by using linear extrapolations and the boundary condition.

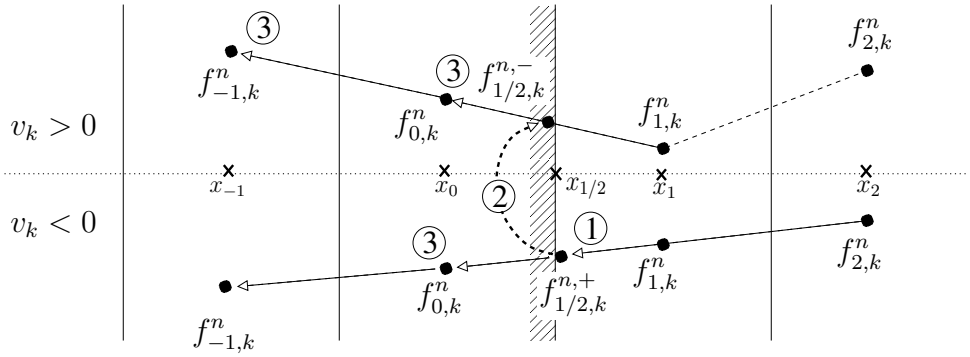

Figure 2: Finite volume scheme with the Yee flux limiter: definition of the ghost cell values $f^n_{0,k}$ and $f^n_{-1,k}$ by using linear extrapolations and the boundary condition.

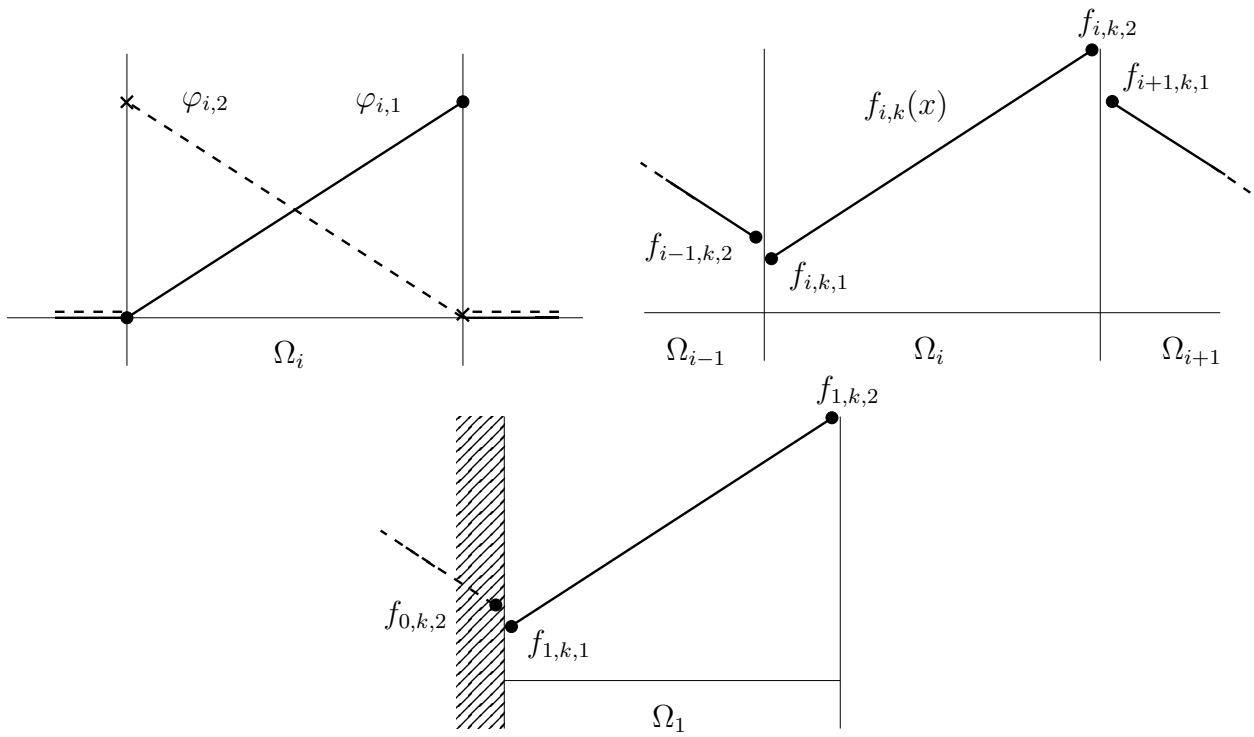

Figure 3: Piecewise linear basis functions (left), piecewise linear approximation of f_k (right), solution at the wall (bottom).

Plates temperature	273 K
Left plate velocity	0 m.s^{-1}
Right plate velocity	300 m.s^{-1}
Distance between the plates	1 m

Gas nature	Argon
m	$0,663.10^{-25}$ kg
R	$208,24$ J.kg^{-1}.K^{-1}
μ_0	$2,117.10^{-5}$ Pa.s
T_0	$273,15$ K
ω	0,81
α	1
Kn	$9,25.10^{-3}$

Table 2: 1D Couette flow: flow parameters and gas properties

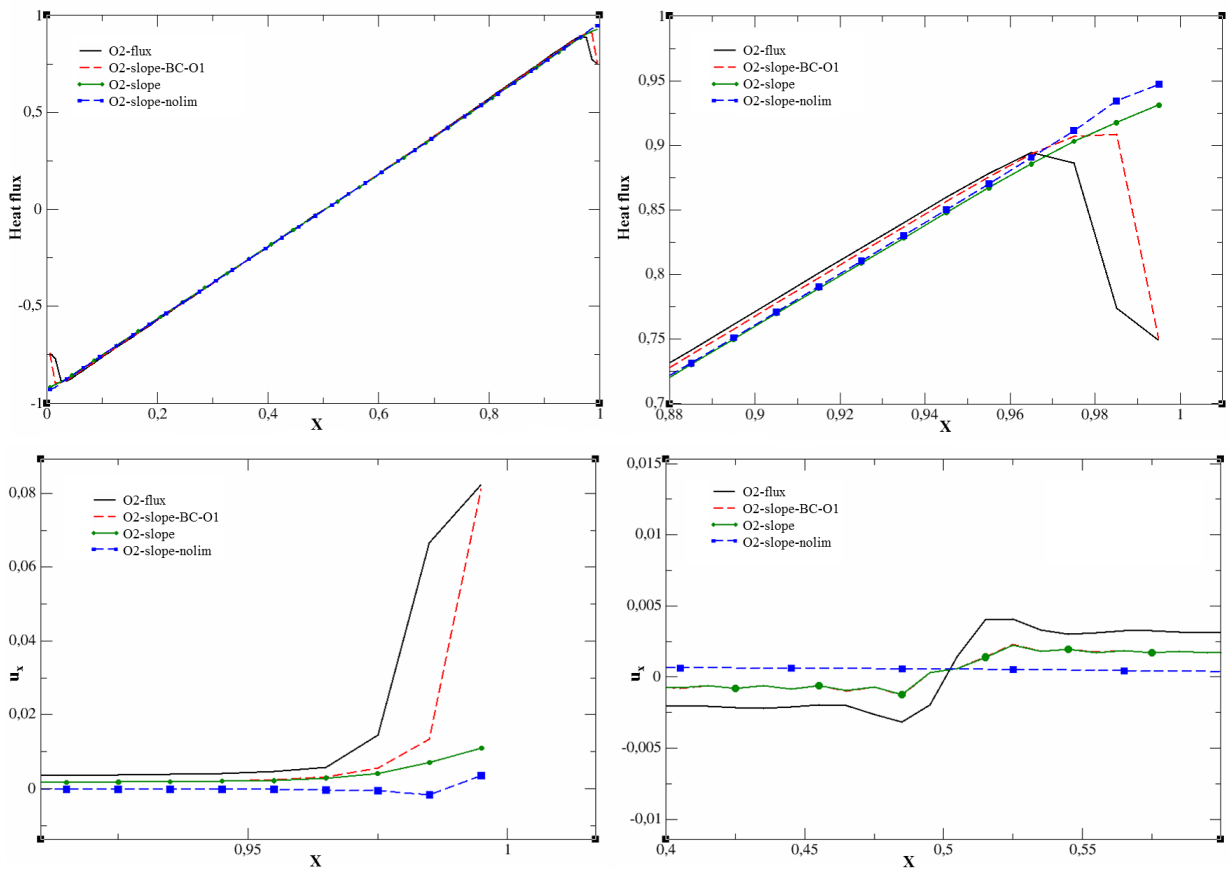

Figure 4: 1D Couette flow: heat flux and horizontal velocity obtained with the different second order schemes: (top left) heat flux, (top right) heat flux, zoom at the moving wall, (bottom left) horizontal velocity, zoom at the moving wall, (bottom right) horizontal velocity, zoom in the middle of the domain.

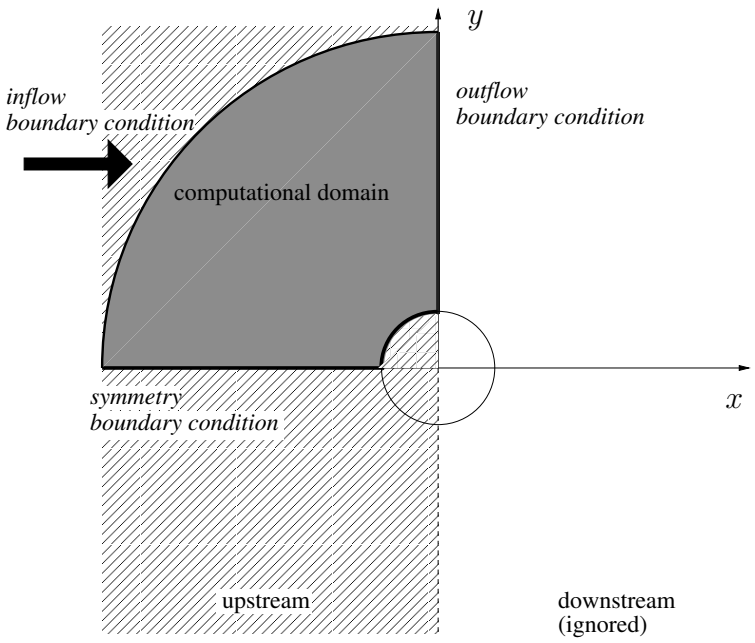

Figure 5: 2D supersonic flow around a cylinder: geometry of the test case.

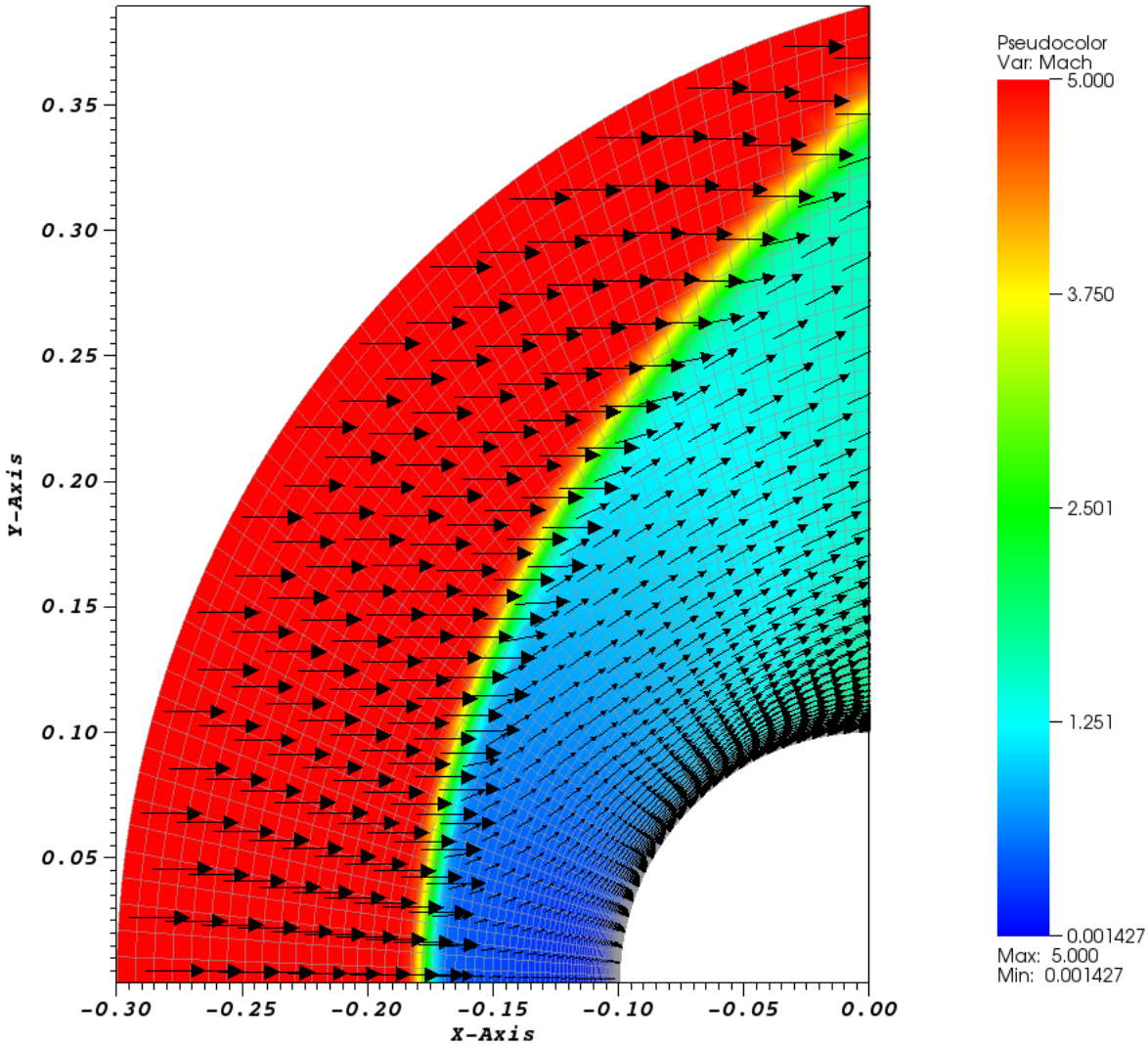

Figure 6: 2D supersonic flow: velocity and Mach number fields (finite volume scheme with slope limiters). The mesh used for the simulation is shown in grey lines.

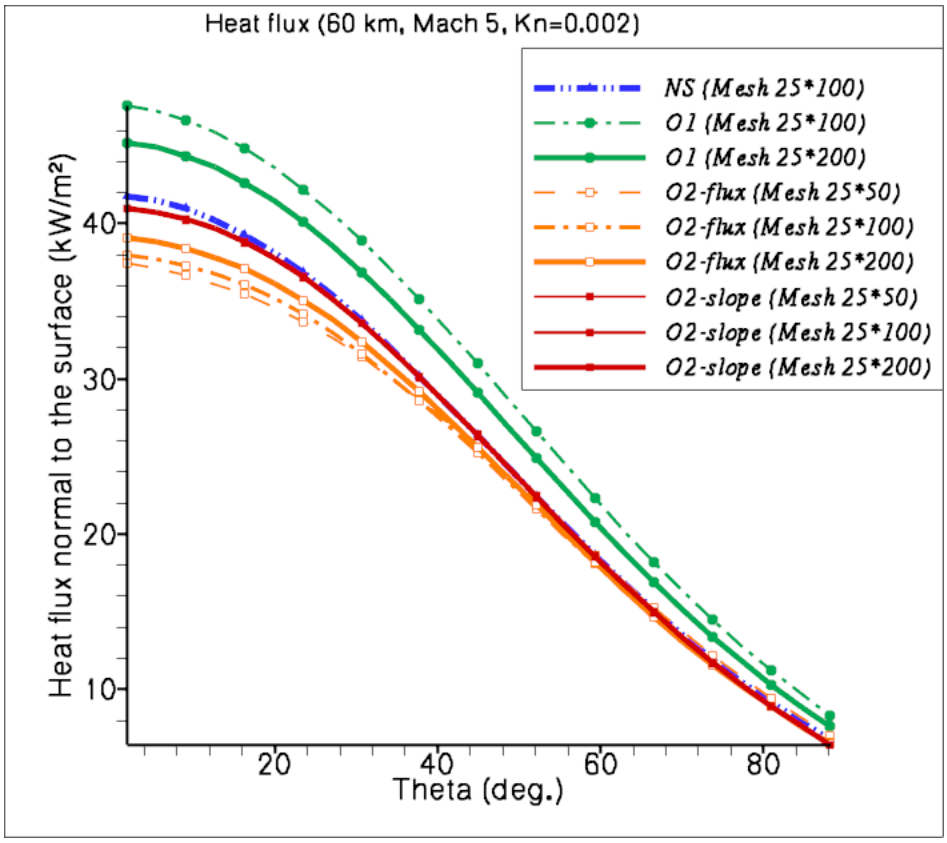

Figure 7: 2D supersonic flow: comparison of the heat flux between BGK solved with finite volume schemes (O1, O2-flux, O2-slope) for different meshes, and Navier-Stokes (NS). Profile of the normal heat flux along the solid wall.

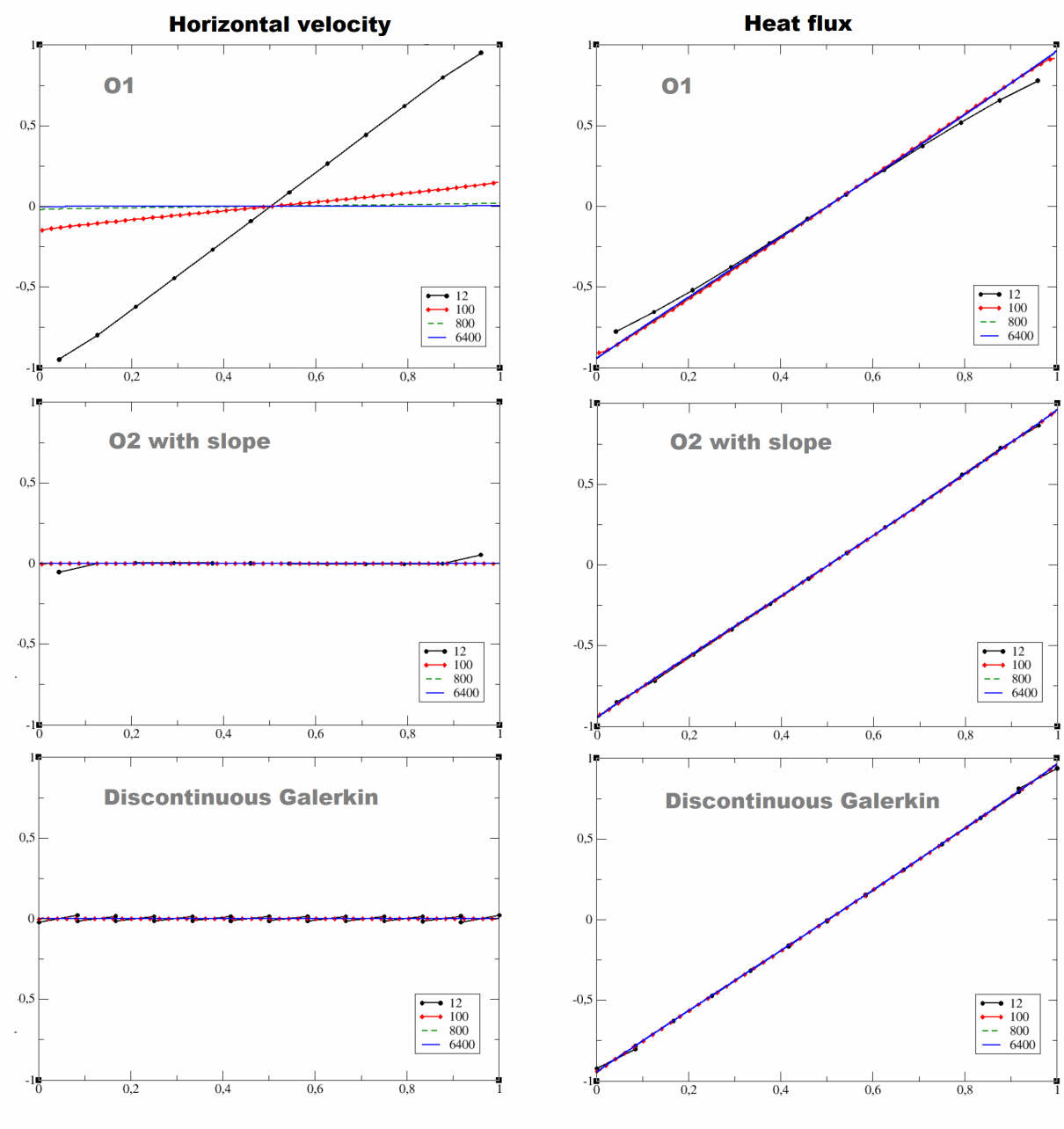

Figure 8: 1D Couette flow: results obtained with the discontinuous Galerkin scheme and first and second order finite volume schemes for the horizontal velocity and the heat flux, with 12 to 6400 grid points.

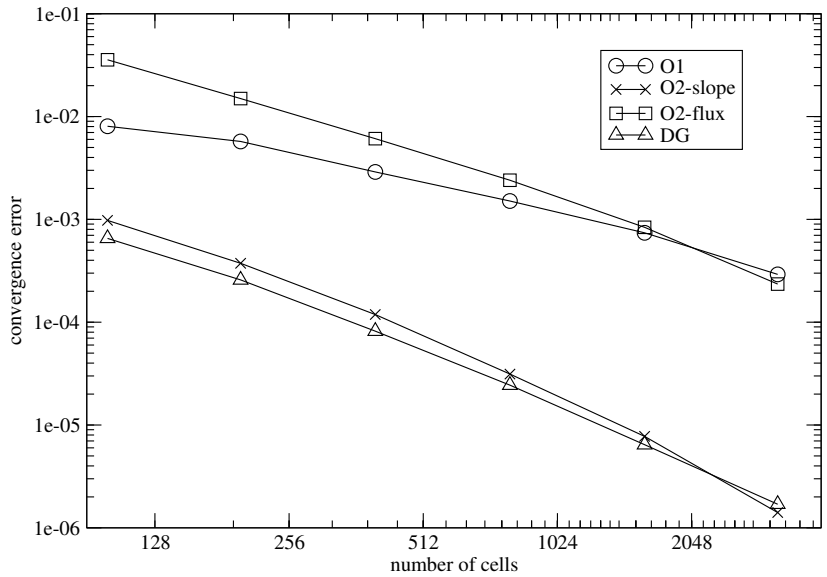

Figure 9: 1D Couette flow: mesh convergence (L^2 norm) of the discontinuous Galerkin and finite volume schemes with uniform meshes, for the heat flux.